Oxygen Doping Modifies Near-Infrared Band Gaps in Fluorescent Single-Walled Carbon Nanotubes

Saunab Ghosh,[1] Sergei M. Bachilo,[1] Rebecca A. Simonette,[2] Kathleen M. Beckingham,[2] R. Bruce Weisman[1]*

Controlled chemical modifications of single-walled carbon nanotubes (SWCNTs) that tune their useful properties have been sought for multiple applications. We found that beneficial optical changes in SWCNTs resulted from introducing low concentrations of oxygen atoms. Stable covalently oxygen-doped nanotubes were prepared by exposure to ozone and then light. Treated samples showed distinct, structure-specific near-infrared fluorescence at wavelengths 10 to 15% longer than displayed by pristine semiconducting SWCNTs. Dopant sites harvest light energy absorbed in undoped nanotube regions by trapping mobile excitons. The oxygen-doped SWCNTs are much easier to detect and image than pristine SWCNTs because they give stronger near-infrared emission and do not absorb at the shifted emission wavelength.

One of the most remarkable characteristics of single-walled carbon nanotubes (SWCNTs) is their diversity of well-defined electronic and optical properties (*1*, *2*). Each SWCNT is composed of covalently bonded carbon atoms forming an ordered tubular structure with a specific diameter and roll-up angle, uniquely defined by a pair of integers called the (*n*,*m*) index. About two-thirds of SWCNT structures are semiconducting. Their intrinsic band gaps are determined by quantum confinement and linked to physical structure, with only slight alterations possible through environmental perturbation.

A variety of optical and electronic applications would benefit from the controlled modification of SWCNT band gaps in bulk samples, individual nanotubes, and even segments within nanotubes. Covalent sidewall reactions have been used to bond nanotubes to chemical groups having a range of selected electronic properties (*3*, *4*). However, to date such reactions have randomly eroded the highly ordered nanotube π-electron structure. The additional covalent bonds remove electrons from the π-system, broadening and suppressing the signature near-infrared (IR) fluorescence peaks of semiconducting SWCNTs (*5*). Here, we describe a different type of chemically modified SWCNT that is more analogous to dopant-tuned semiconductor materials. These stable and easily prepared oxygen-doped nanotubes are near-IR fluorophores that display distinct, structure-specific optical properties systematically shifted from those of the pristine parent. They are more readily detected than pristine nanotubes.

We produce these modified SWCNTs by exposing aqueous suspensions of pristine SWCNTs to low doses of ozone and then photolyzing the resulting product (*6*). Our studies rely on samples highly enriched in individual semiconducting (*n*,*m*) species through nonlinear density gradient ultracentrifugation (*7*). The simpler optical spectra of these sorted samples allow monitoring of the conversion reaction by fluorescence spectroscopy. Immediately after mild ozone exposure, the characteristic near-IR E_{11} fluorescence band shows small red shifts (~0.2) and appreciable broadening (~5%). Subsequent exposure to light induces a new emission feature, termed E_{11}*, that is red-shifted from E_{11}. Spectra measured during this transformation are shown for a (6,5)-enriched sample in Fig. 1A. During phototransformation by light from a desk lamp, 980-nm E_{11} emission diminishes as the 1120-nm E_{11}* feature increases (Fig. 1, A and B). However, except for some broadening, the absorption spectrum remains essentially unchanged by this conversion (Fig. 1C). The transformed nanotubes show very little absorption at their new emission peak, unlike pristine SWCNTs. We estimate that the photoconversion efficiency is quite low, requiring 10^7 to 10^9 absorbed photons per micrometer of SWCNT length. An excitation-emission contour plot demonstrates that near-IR emission from both the original and the transformed (6,5) sample is induced by absorption at the same E_{22} transition (Fig. 1D). The shifted emission from our converted SWCNTs differs in wavelength from the weak intrinsic satellite features observed in pristine samples (*8*–*10*). In addition to the prominent shifted emission band, a weak secondary shifted feature can also be seen (*6*).

Very low ozone doses followed by photoconversion are required to prepare such modified SWCNTs. They are qualitatively different from those prepared through more extensive nanotube ozonation (*11*–*17*), which quenches SWCNT near-IR fluorescence (*18*). Of several ionic surfactants used to suspend samples during ozonation treatment, we found that sodium tridecylbenzenesulfonate (STBS) gave the most reproducible results, presumably because it could be used at lower concentrations that compete less for reaction with ozone. Resonance Raman spectra revealed that the ozone-and-photolysis transformation was accompanied by the appearance of a sharp D-band near 1310 cm^{-1} (figs. S10 and S11) signifying covalent functionalization of the nanotube sidewall (*19*). The transformation reaction also occurred, although less efficiently, when weaker oxidants H_2O_2 or K_2CrO_4 were substituted for ozone (fig. S18) (*6*). We conclude that the transformed nanotubes incorporate covalently bonded oxygen. Similar but unintended oxidation may have led to the defect-induced emission reported from some individual SWCNTs exposed to intense pulsed laser light (*20*).

Other semiconducting (*n*,*m*) species also underwent oxygen doping. For example, bulk samples enriched in (6,4) and (8,3) showed reduced E_{11} emission and the growth of a new red-shifted E_{11}* emission band as they were treated with ozone and visible light (fig. S9). Spectral transformations were less efficient for larger-diameter SWCNTs (fig. S15) (*6*). We measured spectral positions and widths of E_{11}* peaks from 10 different oxygen-doped (*n*,*m*) species in STBS for comparison with their pristine forms (Table 1). The spectral red shifts between E_{11} and E_{11}* ranged from 106 to 214 meV and showed a strong positive correlation with E_{11} (Fig. 1E) (*21*). These doping-induced shifts represent optical band gap decreases of 10 to 15% from the pristine values.

Spectroscopic measurements on individual nanotubes revealed photophysical heterogeneity in the doped samples. The results are illustrated with fluorescence spectra acquired from three individual nanotubes in a (6,5)-enriched bulk sample (Fig. 2A). One nanotube was pristine and

[1]Department of Chemistry and R. E. Smalley Institute for Nanoscale Science and Technology, Rice University, Houston, TX 77005, USA. [2]Department of Biochemistry and Cell Biology and R. E. Smalley Institute for Nanoscale Science and Technology, Rice University, Houston, TX 77005, USA.

*To whom correspondence should be addressed. E-mail: weisman@rice.edu

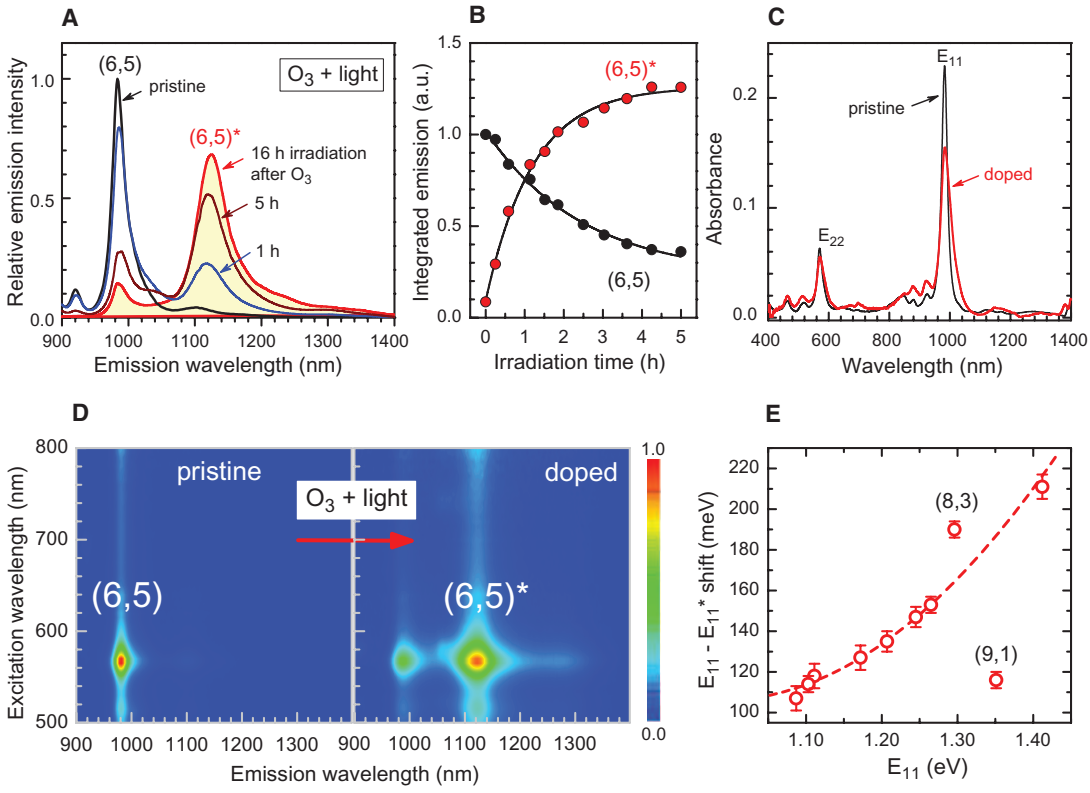

Fig. 1. Spectral changes in a (6,5)-enriched SWCNT dispersion exposed to ozone and light. (**A**) Emission spectra measured with 785-nm excitation after a single treatment with ozone and 1 to 16 hours of white-light irradiation. (**B**) Spectrally integrated emission under the (6,5) main band (black) and side band (red) versus irradiation time with a desk lamp. (**C**) Absorption spectra (path length 1 cm) of the SWCNT sample before (black) and after (red) treatment with ozone and light. (**D**) Photoluminescence excitation-emission contour plots from the (6,5)-enriched sample before and after treatment. The (6,5)* emission feature shows the same excitation peak wavelength as the (6,5) feature. (**E**) Measured photon energy differences between the unshifted and shifted fluorescence peaks of 10 different bulk (*n*,*m*) species as a function of unshifted emission energy. Points show experimental data; the dashed line is a quadratic function drawn to guide the eye. Two points far from the line are labeled with their (*n*,*m*) values.

the other two had been oxygen-doped. One of the two doped nanotubes showed an intense shifted emission band and nearly complete depletion of the normal band; the other emitted both shifted and normal bands with similar peak intensities. These observations demonstrate that the extent of oxygen doping can vary among nanotubes within the same bulk sample. Moreover, the bimodal emission traces imply that individual nanotubes can contain both pristine and doped regions with independent fluorescence spectra. We have compared the polarization of E_{11} and E_{11}* emission from an individual SWCNT whose spectrum is shown in Fig. 2A. The integrated intensities of the two bands measured through a linear polarizer both follow a $\cos^2$ pattern with matching phase angles (Fig. 2B). This result demonstrates that E_{11}* emission arises from a transition dipole oriented parallel to that of the normal E_{11} emission, which is known to lie along the nanotube axis.

Oxygen-doped SWCNTs showed good stability. Transformed bulk samples have been stored under ambient conditions for several months with no change in spectral properties. To check photostability, we measured the E_{11}* emission spectrum of an individual doped (6,4) nanotube at 1-min intervals while irradiating it with 775-nm light at 150 W/cm^2. The emission remained constant in peak position and shape but showed a slight (~3%) decrease in intensity over the 10-min irradiation period (Fig. 2C). The E_{11}* emission intensity remained proportional to excitation intensity at levels up to several kW/cm^2 (fig. S20).

Table 1. Comparative spectral characteristics of pristine and oxygen-doped SWCNTs (*35*). Precise E_{11}* peak positions depend on the extent of doping.

(*n*,*m*)	Pristine E_{11} peak (nm)	Treated E_{11} peak (nm)	Treated E_{11}* peak (nm)	Treated E_{11}-E_{11}* shift (meV)	Pristine E_{11} width (meV)	Treated E_{11} width (meV)	Treated E_{11}* width (meV)
(6,4)	878	889	1050	214	35	45	77
(7,3)	996	1012	1150	147	34	39	75
(9,1)	918	924	1012	117	26	43	73
(6,5)	980	983	1120	154	28	43	50
(8,3)	957	960	1125	189	26	31	48
(9,2)	1141	1147	1272	106	25	28	62
(7,5)	1027	1033	1155	127	23	41	56
(8,4)	1116	1125	1258	117	24	42	72
(10,2)	1058	1070	1190	117	22	24	56
(7,6)	1124	1135	1266	113	28	45	80

We propose a photophysical model in which oxygen doping of a SWCNT at low doses creates sparse perturbed regions that have locally reduced band gaps. Because the great majority of carbon atoms are remote from the doping sites, the overall absorption spectrum remains nearly unchanged and shows no appreciable component at the E_{11}* emission wavelength. However, excitons generated by light absorption in undoped regions are mobile, as in pristine nanotubes (*22*–*24*), and may diffuse during their lifetimes to doped sites where they are stabilized by the local potential minimum. Radiative recombination of these trapped excitons gives the E_{11}* emission characteristic of the doped nanotubes. A single treated nanotube may show both E_{11} and E_{11}* emission because excitons can radiate in pristine or doped locations. Higher doping levels increase the E_{11}*/E_{11} intensity ratio by raising the probability of trapping before emission. Assuming irreversible trapping and mean exciton ranges somewhat below pristine values, we estimate that SWCNTs with intensity ratios near 1 contain approximately one oxygen atom per few thousand carbon atoms.

We used quantum chemical modeling to predict the most stable product of O_3 reaction with SWCNTs and the resulting wave function perturbations over nanotube segments 2 to 3 nm in length, representing the axial size of an exciton

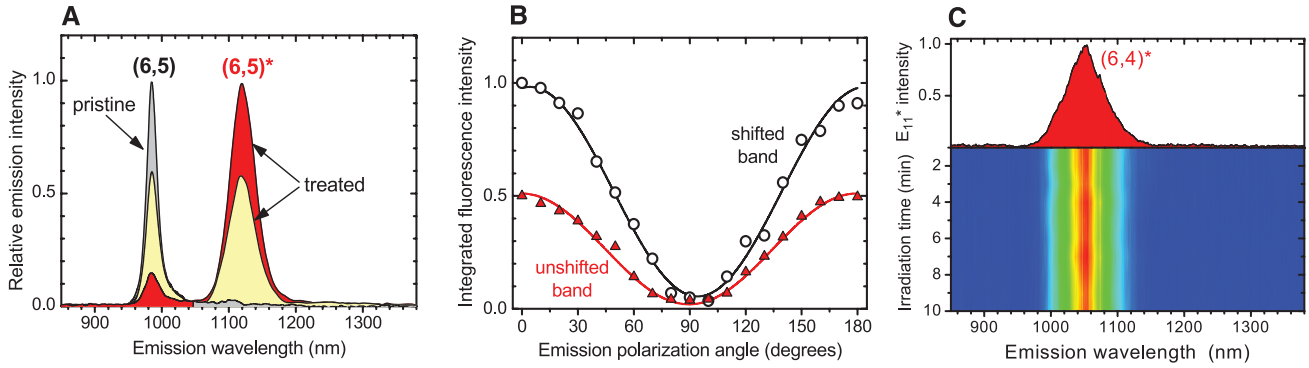

Fig. 2. Spectral characterization of individual oxygen-doped SWCNTs. (**A**) Fluorescence emission spectra of three individual (6,5) nanotubes. The gray trace is from a pristine SWCNT; the red and yellow traces are from different treated nanotubes in the same bulk sample. (**B**) Spectrally integrated intensities from the nanotube giving the yellow trace in (A) as a function of emission polarization angle. (**C**) Emission spectrum (top) and contour plot of successive emission spectra (bottom) from a single heavily treated (6,4) SWCNT continuously irradiated at an intensity of 150 W/cm^2. Spectra were acquired each minute.

(*25*, *26*). Such segments include ~200 carbon atoms, making them very challenging subjects for ab initio studies. We therefore applied a semi-empirical model (PM3) instead. In agreement with previous reports (*27*–*30*), our computations point to formation of an ozonide adduct in which O_3 covalently bridges two adjacent carbon atoms (Fig. 3A, left). Exothermicities vary from 20 to 40 kcal/mol, depending on SWCNT species and orientation of the O_3 addend (fig. S2). The most stable adducts predicted for smaller-diameter nanotubes tend to have O_3 groups oriented nearly parallel to the tube axis. In a process analogous to that experimentally observed in fullerene ozonides (*31*–*33*), subsequent loss of O_2 from the ozonide leaves an epoxide with an oxygen atom bridging the same adjacent sp^3 carbon atoms (Fig. 3A, center). However, our calculations show this epoxide adduct to be less stable [by more than 20 kcal/mol for a (6,5) nanotube] than an isomer in which the oxygen atom links two sp^2 carbon atoms nearly perpendicular to the nanotube axis through C-O-C ether bonds (Fig. 3A, right). We propose that the light-induced step in our treatment is irreversible photoisomerization of the epoxide adduct into this much more stable ether structure. Similar results for the relative stabilities of SWCNT oxide isomers were recently reported by Johnson and co-workers from density functional theory (DFT) ab initio calculations (*28*).

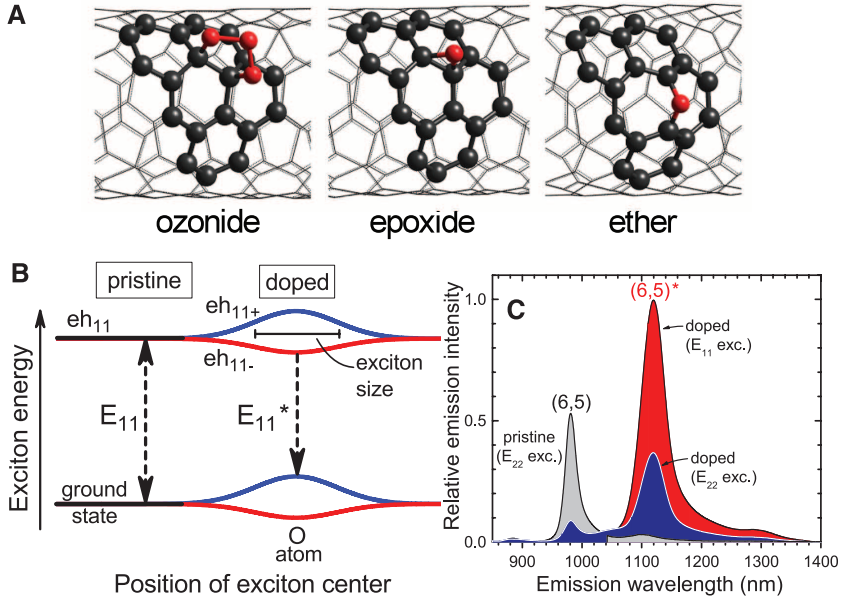

Fig. 3. (**A**) PM3-computed structures of the most stable ozonide (left), epoxide (center), and ether (right) adducts of a segment of (6,5) SWCNT. (**B**) Sketch of qualitative energy levels, showing oxygen-induced perturbations to the ground and lowest "bright" exciton states as a function of axial distance from the dopant atom. Dashed arrows indicate relevant allowed optical transitions. (**C**) Bulk emission spectra of (6,5) SWCNTs: a pristine sample excited at its E_{22} absorption (gray), an oxygen-doped sample excited at its E_{22} absorption (blue), and the same oxygen-doped sample excited at its E_{11} absorption (red).

The two oxide isomers cause quite different perturbations to the nanotube π-electron system. In the epoxide adduct, both carbon atoms bonded to the oxygen are converted to sp^3 hybridization, and five C-C bonds are appreciably lengthened and angularly distorted. By contrast, in the ether adduct, sp^2 carbon hybridization is maintained, only one C-C bond lengthens (the broken one under the ether bridge), and angular distortions are smaller. The electronic and spectroscopic characters of the ether adduct should be much more similar than the epoxide to the pristine SWCNT. An analogous result was demonstrated in earlier experimental studies of C_{60} and C_{70} treated with ozone (*31*, *32*, *34*). After the initially formed fullerene ozonides lost O_2 to form oxides, those with ether bridges and sp^2 carbon hybridization could be distinguished from fullerene epoxides because they resembled the pristine parent fullerene in electronic absorption spectroscopy. Optical excitation of several C_{70} oxides converted them into other isomers through shifts of the oxygen atom on the cage surface (*32*). We propose that the light-induced process observed in our treated SWCNTs is a related photoisomerization.

A comparison of computed wave functions for doped and pristine SWCNTs helps us to interpret the observed optical properties. The highest occupied and lowest unoccupied molecular orbitals (HOMO and LUMO) for a perfect, infinitely long semiconducting SWCNT are both doubly degenerate. To model the optical perturbations caused by sparse doping, we considered short SWCNT segments having lengths comparable to exciton sizes (a few nanometers). For such segments, the degenerate HOMO and LUMO orbitals of chiral nanotubes show a small end-effect splitting on the order of 0.01 meV. By contrast, an ether group oriented across the tube axis induces a far larger perturbation of 100 to 200 meV (figs. S4, S7, and S8). This splits the ground-state and excited-state (eh_{11}) energies in the vicinity of the doping site to give four distinct levels (Fig. 3B). Dipole selection rules allow optical transitions between the upper excited-state sublevel and the lower ground-state sublevel, and also between the lower excited-state and upper ground-state sublevels. The latter transition repre-

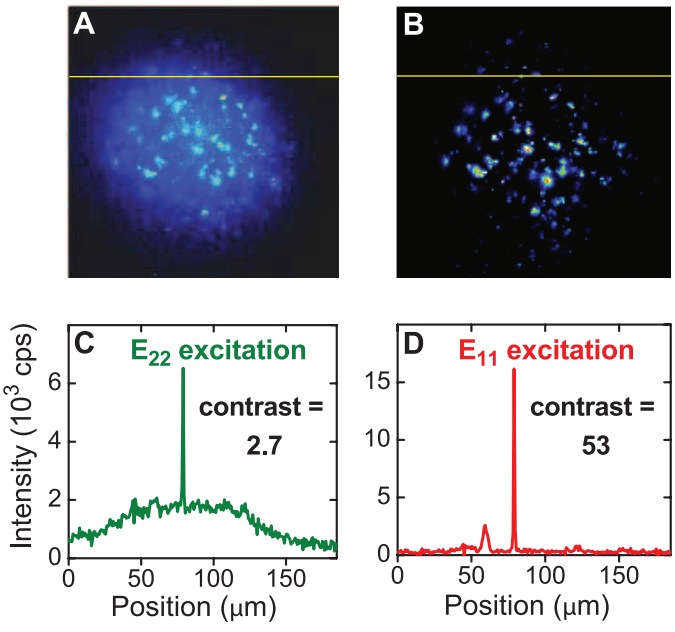

Fig. 4. Comparative near-IR fluorescence micrographs (100-ms exposures) of a cultured human uterine adenocarcinoma cell specimen containing oxygen-doped (6,5) SWCNTs. (**A** and **B**) Excitation was at the E_{22} transition (A) and the E_{11} transition (B) under matched conditions. (**C** and **D**) Intensity profiles and peak/background contrast ratios along the yellow horizontal lines in the images. The sharp peaks near 80 μm are from a single nanotube.

sents the red-shifted fluorescence (E_{11}*) observed from oxygen-doped SWCNTs. Our calculations also predict that the allowed transition dipoles remain parallel to the nanotube axis, in agreement with polarization measurements (Fig. 2B).

Absorption spectroscopy of our lightly doped nanotubes reveals neither of the distinctly shifted, allowed transitions between split levels because the strong electronic perturbation from oxygen doping is local and affects only a small fraction of the carbon atoms. However, we observe broadening of E_{11} and E_{22} absorptions, probably from a distribution of small excitonic energy shifts extending to longer distances from doping sites. After light absorption, some of the excitons from undoped regions diffuse to doped centers, become trapped by the reduced potential, and emit in the red-shifted (E_{11}*) transition involving the lower LUMO and upper HOMO components. Trapping will be reversible if the potential well is not deep relative to the thermal energy k_BT, and the ratio of E_{11}* to E_{11} emission intensities will decrease as temperature increases. We measured these ratios over a limited temperature range and constructed van't Hoff plots to deduce well depths of 40 meV for (8,3) and 61 meV for (6,5) (fig. S12) (*6*). Consistent with the sketch of Fig. 3B, these values are less than half of the red shift between E_{11}* and E_{11} peaks because they represent only the trapping energy, (the difference between the levels marked eh_{11} and eh_{11-}). By assuming that the E_{11}*/E_{11} intensity ratio reflects an equilibrium distribution of exciton locations, we estimate a carbon/oxygen ratio of ~2000 for (6,5) SWCNTs with equal emission intensities (*6*).

After light energy is harvested throughout the nanotube by strong E_{11} and E_{22} absorption bands comparable to those of pristine SWCNTs, mobile excitons transfer the absorbed energy to doping sites that can emit red-shifted E_{11}* fluorescence. This spectral separation of intense near-IR absorption and emission, which is absent in pristine SWCNTs, allows greatly improved optical imaging and detection of the doped nanotubes. Three factors contribute. First, excitation light can be tuned to a sample's E_{11} peak, which has greater absorptivity than the E_{22} peak that must be excited in a pristine sample. Second, emission efficiency is also improved, as spectrally integrated E_{11}* emission exceeds E_{11} emission of the pristine SWCNT under equivalent excitation conditions. These differences are illustrated by three spectra recorded from the same (6,5)-enriched sample excited at its E_{22} peak before doping, at its E_{22} peak after doping, and at its E_{11} peak after doping (Fig. 3C). The third factor is that excitation with longer-wavelength, near-IR light generates far less background emission from biological or environmental specimens.

We demonstrated this enhanced detectivity by near-IR fluorescence microscopy of cultured human uterine adenocarcinoma cells incubated in growth medium containing oxygen-doped (6,5) SWCNTs coated with Pluronic F127 surfactant. For comparison, 100-ms fluorescence images of the same specimen were recorded using E_{22} excitation (as for pristine samples) and E_{11} excitation of matched intensity. Optical filters blocked wavelengths below 1050 nm in the imaging path. The resulting images are shown (false-colored) in Fig. 4, A and B, along with intensity profile plots along the horizontal lines drawn through the image frames (Fig. 4, C and D). Most individual spots represent single nanotubes. The profile plots show that E_{11} excitation provides more than 3 times the emission intensity with one-sixth the background level compared to E_{22} excitation. This improves image contrast by a factor of ~20.

Oxygen doping of SWCNTs is a simple chemical treatment that spectrally separates near-IR emission from absorption bands. This makes doped SWCNTs superior near-IR fluorophores and suggests the prospect of a family of near-IR SWCNT lasers pumped by optical excitation, energy transfer, or charge injection.

References and Notes

1. S. Reich, C. Thomsen, J. Maultzsch, *Carbon Nanotubes: Basic Concepts and Physical Properties* (Wiley-VCH, Weinheim, 2004).
2. S. M. Bachilo *et al.*, *Science* **298**, 2361 (2002); 10.1126/science.1078727.
3. S. Banerjee, T. Hemraj-Benny, S. S. Wong, *Adv. Mater.* **17**, 17 (2005).
4. A. Hirsch, O. Vostrowsky, *Top. Curr. Chem.* **245**, 193 (2005).
5. S. Qin *et al.*, *Macromolecules* **37**, 3965 (2004).
6. See supporting material on *Science* Online.
7. S. Ghosh, S. M. Bachilo, R. B. Weisman, *Nat. Nanotechnol.* **5**, 443 (2010).
8. O. Kiowski, K. Arnold, S. Lebedkin, F. Hennrich, M. M. Kappes, *Phys. Rev. Lett.* **99**, 237402 (2007).
9. Y. Murakami *et al.*, *Phys. Rev. B* **79**, 195407 (2009).
10. O. N. Torrens, M. Zheng, J. M. Kikkawa, *Phys. Rev. Lett.* **101**, 157401 (2008).
11. D. B. Mawhinney *et al.*, *J. Am. Chem. Soc.* **122**, 2383 (2000).
12. S. Banerjee, S. S. Wong, *J. Phys. Chem. B* **106**, 12144 (2002).
13. L. T. Cai, J. L. Bahr, Y. X. Yao, J. M. Tour, *Chem. Mater.* **14**, 4235 (2002).
14. Z. Chen, K. J. Ziegler, J. Shaver, R. H. Hauge, R. E. Smalley, *J. Phys. Chem. B* **110**, 11624 (2006).
15. D. Ogrin, J. Chattopadhyay, A. K. Sadana, W. E. Billups, A. R. Barron, *J. Am. Chem. Soc.* **128**, 11322 (2006).
16. J. M. Simmons *et al.*, *J. Phys. Chem. B* **110**, 7113 (2006).
17. M. Li, M. Boggs, T. P. Beebe, C. P. Huang, *Carbon* **46**, 466 (2008).
18. K. Tsvaygboym, thesis, Rice University (2007).
19. See fig. S9 for additional Raman data.
20. H. Harutyunyan *et al.*, *Nano Lett.* **9**, 2010 (2009).
21. Positions of shifted peaks depend somewhat on extent of doping.
22. L. Cognet *et al.*, *Science* **316**, 1465 (2007).
23. A. J. Siitonen, D. A. Tsyboulski, S. M. Bachilo, R. B. Weisman, *Nano Lett.* **10**, 1595 (2010).
24. A. J. Siitonen, D. A. Tsyboulski, S. M. Bachilo, R. B. Weisman, *J. Phys. Chem. Lett.* **1**, 2189 (2010).
25. V. Perebeinos, J. Tersoff, Ph. Avouris, *Phys. Rev. Lett.* **92**, 257402 (2004).
26. L. Lüer *et al.*, *Nat. Phys.* **5**, 54 (2009).
27. S. Picozzi, S. Santucci, L. Lozzi, L. Valentini, B. Delley, *J. Chem. Phys.* **120**, 7147 (2004).
28. W. L. Yim, J. K. Johnson, *J. Phys. Chem. C* **113**, 17636 (2009).
29. X. Lu, L. Zhang, X. Xu, N. Wang, Q. Zhang, *J. Phys. Chem. B* **106**, 2136 (2002).
30. B. Akdim, T. Kar, X. Duan, R. Pachter, *Chem. Phys. Lett.* **445**, 281 (2007).
31. D. Heymann *et al.*, *J. Am. Chem. Soc.* **122**, 11473 (2000).
32. D. Heymann, S. M. Bachilo, R. B. Weisman, *J. Am. Chem. Soc.* **124**, 6317 (2002).
33. D. Heymann, R. B. Weisman, *C. R. Chim.* **9**, 1107 (2006).
34. R. B. Weisman, D. Heymann, S. M. Bachilo, *J. Am. Chem. Soc.* **123**, 9720 (2001).
35. Samples suspended in aqueous sodium tridecylbenzenesulfonate.

36. Supported by NSF grant CHE-0809020, Welch Foundation grants C-0807 and C-1119, and NASA grant NNX09AH43G. We thank J. K. Johnson for unpublished computational results, and C. Farach-Carson and D. Carson for providing the cultured cell line.

Supporting Online Material

www.sciencemag.org/cgi/content/full/science.1196382/DC1
Materials and Methods
Figs. S1 to S20
Table S1
References

11 August 2010; accepted 14 October 2010
Published online 25 November 2010;
10.1126/science.1196382